I&EC research
Industrial & Engineering Chemistry Research

pubs.acs.org/IECR

Article

CO_2 Reforming of CH_4 over SiO_2-Supported Ni Catalyst: Effect of Sn as Support and Metal Promoter

Giuseppe Pantaleo, Valeria La Parola,* Maria Luisa Testa, and Anna Maria Venezia*

Cite This: *Ind. Eng. Chem. Res.* 2021, 60, 18684−18694

Read Online

ACCESS | Metrics & More | Article Recommendations | Supporting Information

ABSTRACT: Ni (10 wt %) catalysts supported on SiO_2 and on SiO_2 doped with 1 and 4 wt % Sn and a Sn-doped Ni catalyst supported on silica were prepared by microwave-assisted precipitation methods. The catalysts, analyzed by TPR, XRD, and XPS techniques, were tested in the dry reforming of methane (DRM) with CO_2. The reaction was conducted at atmospheric pressure in a temperature range of 450−800 °C with a feed gas mixture containing CH_4 and CO_2 in a 1:1 ratio in He. The effect of the catalyst pre-reduction temperatures of 550 and 750 °C was considered. As compared to the bare Ni−SiO_2 catalysts, doping silica with 4 wt % Sn, corresponding to a Sn/Ni molar ratio of 0.2, substantially decreased the amount of deposited carbon but determined a consistent loss of activity. In the presence of a lower amount of tin (Sn/Ni = 0.05), with a lower amount of formed carbon, the catalyst was still less active and less stable as compared to bare Ni−SiO_2. On the contrary, changing the sequence of metal addition, i.e., adding 1 wt % Sn to Ni−SiO_2, slightly improved the activity and the catalytic stability at 650 °C during 24 h on stream, also reducing the carbon formation. The structural characterizations before and after the reaction were in accord with a better structural stability of the nickel particle when doped by tin. The nickel ensemble dilution upon Ni_xSn_y alloy formation, as detected by XRD, hindered formation of surface carbon.

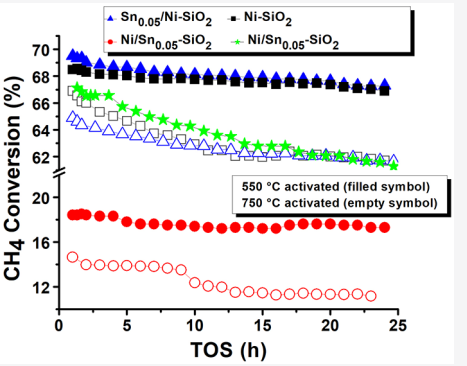

1. INTRODUCTION

The catalytic reaction of dry reforming of methane (DRM) with CO_2, leading to the production of syngas, has gained increasing industrial attention. One of the reasons for this renewed interest concerns with the larger availability of reservoir of methane as compared to the depleting crude oil reserve.[1] Moreover, the suggested use of the biogas (CH_4/CO_2 mixtures) arising from waste materials, such as municipal waste, sewage sludge, and agricultural waste, as the main feedstock for the reaction makes the process even more interesting. In addition to these motivations, as compared to other methane reforming processes, a mature DRM technology would contribute to the recycling of CO_2, a strong greenhouse effect gas, naturally present in the earth's atmosphere but the amounts of which are greatly increased by a variety of human activities.[2]

The DRM process involves the reaction

$$CH_4 + CO_2 \rightleftarrows CO + H_2 \quad (\Delta H_{298K} = 247\ kJ/mol) \tag{1}$$

compared to the methane steam reforming (SRM), represented by equation

$$CH_4 + H_2O \rightleftarrows CO + 3H_2 \quad (\Delta H_{298K} = 206\ kJ/mol) \tag{2}$$

DRM produces syngas with lower H_2/CO ratio which is a preferable feedstock for the Fischer−Tropsch synthesis (FTS) of long-chain hydrocarbons and for the synthesis of oxygenates.[3] Therefore, DRM would avoid the adjustment of the H_2/CO ratio by means of the endothermic reverse water gas shift (WGS) reaction:

$$CO_2 + H_2 \rightleftarrows CO + H_2O \quad (\Delta H_{298K} = 41\ kJ/mol) \tag{3}$$

However, a drawback of DRM as compared to SRM is represented by the large formation of carbon mainly due to (i) methane decomposition and (ii) the Boudouard disproportion reaction, described by eqs 4 and 5, respectively:

$$CH_4 \rightarrow C + 2H_2\ (\Delta H_{298K} = +75\ kJ/mol) \tag{4}$$

$$2CO \rightarrow C + CO_2\ (\Delta H_{298K} = -171\ kJ/mol) \tag{5}$$

As seen in eq 1, the DRM reaction is highly endothermic and requires high temperature conditions.[3] At the high temperature of the reaction, the exothermic Boudouard reaction is inhibited. Therefore, coke formation at T > 700 °C mainly proceeds via methane cracking over the active metal

Special Issue: José Luis García Fierro Festschrift

Received: June 7, 2021
Revised: July 18, 2021
Accepted: July 23, 2021
Published: August 3, 2021

atoms. As reported for other reactions involving activation of methane, noble metals would be the most appropriate in terms of coke resistance, easy reducibility, structural stability, and high activity. However, their elevated cost and limited availability hinder their use for industrial application.[2,4] In terms of the cost/efficiency ratio, nickel supported on different oxides are the preferred catalysts for the DRM process, in spite of the fact that nickel catalysts without appropriate precautions suffer from a catalytic instability due to easy deactivation by carbon deposition and nickel particle sintering.[3] It has been suggested that adjusting the acidity−basicity of the catalyst surface or reducing the Ni particle size below 8 nm would reduce the carbon formation.[5,6] As reported in literature and according to DFT calculations, methane decomposition is a structure-sensitive reaction, preferentially occurring on low-coordinated step sites.[7,8] Carbon nucleation and growth preferentially occur on a stepped rather than planar Ni surface.[7] As suggested by theory, by blocking the step sites, carbon deposition can be eliminated, while the catalyst would only have a moderately reduced reforming activity.[9] Supporting the metal on a carrier with Lewis basicity would also inhibit carbon coke formation.[10,6] Indeed, since CO_2 is an acid gas, it will adsorb and then dissociate easily on a basic support, resulting in higher activity and therefore lower carbon formation or, by a different mechanism, it can easily react with the deposited carbon inhibiting carbon accumulation.[3,11] Clear evidence for link between particle sizes and rate of carbon formation have also been reported.[8] Alloying nickel with a noble metal by decreasing the *ensemble size* of the active site is also a way to limit the carbon deposition besides preventing metal sintering. Nevertheless, as underlined above, the elevated cost of noble metals is quite prohibitive, and it is more convenient to develop noble-metal-free catalysts. Among the non-noble metals, Sn seems to be a promising alternative. Several experimental and computational approaches are reported in the literature to explain the effect of the Ni−Sn interaction in both DRM and SRM.[12−15] Most of the reported studies concerned with alumina-supported catalysts showed a stronger interaction between the metals and the support. In general, the bimetallic Sn−Ni systems have shown good resistance to carbon deposition, but at the expense of the reforming activity, pointing out the crucial role of an appropriate Sn/Ni atomic ratio. Some contradictory results have been obtained in the case of silica supported systems, where Sn was shown to have negative effect on the activity and a rather neutral effect on coking.[16] Within this context, the present work aims to develop methane reforming nickel catalysts with superior coke and metal sintering resistance, by preparing bimetallic Sn−Ni catalysts supported over high surface area silica with two different Sn/Ni atomic ratios. A high surface area and inert support such as SiO_2 was chosen in order to maximize the interaction between Ni and Sn aiming to affect the Ni active sites and their catalytic behavior. Moreover, SnO_2 having a fair basicity of its own, when added to the silica support, could contribute to the decrease of the carbon without affecting the activation of methane.[17] By slightly varying the preparation procedure, this study intends to investigate the effect of Sn as either a support modifier or an active site promoter. The DRM activity of the tin-promoted catalysts compared with the activity of the unpromoted nickel catalyst is discussed in terms of structural and electronic properties.

2. EXPERIMENTAL SECTION

2.1. Support and Catalyst Preparation. All the chemicals required to prepare the supports and the catalysts were used without any additional purification and were all obtained from Sigma-Aldrich: tetraethylorthosilicate ($Si(OC_2H_5)_4$, TEOS, 98%), nickel nitrate $Ni(NO_3)_2{\cdot}6H_2O$, 99.9%, tin chloride $SnCl_2{\cdot}2H_2O$, 99.95%, ethanol, and tetrahydrofuran C_4H_8O (THF).

High-surface-area silica was prepared according to a previously reported sol−gel method using TEOS as precursor.[18] Hydrolysis of TEOS occurred under acid conditions at pH 5 with acetic acid, followed by condensation. The gel was dried at 110 °C and calcined at 450 °C for 4 h. Silica with a specific surface area of 690 m^2/g was obtained.

Microwave activation was chosen for the preparation of the doped supports and nickel catalysts. Indeed, as described in the literature the use of microwaves during material synthesis provides uniform heating of the precursors and consequently helps to reduce the reaction time, lowers the reaction temperatures, and improves the properties of the final products in terms of homogeneity and particle size.[18,19] The supports with 4 and 1 wt % Sn were prepared by impregnating the lab-made SiO_2 with an appropriate volume of a 0.01 M solution of $SnCl_2$ in THF. The obtained suspension was placed inside a conventional household microwave set at 180 W power and operated in 30 s cycles (on for 20 s, off and stirring for 20 s) for a total time of 20 min and irradiation time of 10 min. The activated suspension was dried overnight inside a heating mantle set at 60 °C. Thereafter, the solid was calcined at 500 °C for 2 h with a heating rate of 5 °C/min. The supports were labeled as $Sn_{4wt\%}-SiO_2$ and $Sn_{1wt\%}-SiO_2$ respectively.

Nickel catalysts with 10 wt % Ni, supported on pure silica and on SiO_2 doped with different amounts of tin, were prepared by microwave-assisted precipitation. The procedure consisted of adding 10 mL of an aqueous solution of $Ni(NO_3)_2{\cdot}6H_2O$ of an appropriate concentration to a suspension of silica or of Sn-doped silica in 20 mL of ethanol. Nickel hydroxide was precipitated by dropwise adding 10% (*v*/*v*) NH_4OH solution until pH 9. The suspension underwent the same treatment with microwaves as described above for the supports. After filtration, the collected precipitate was washed with distilled water and ethanol, dried at 100 °C for 1 h, and then calcined at 650 °C for 1 h with a heating rate of 5 °C/min. The monometallic catalyst was labeled as $Ni-SiO_2$, and the two bimetallic ones with molar ratios Sn/Ni = 0.20 and 0.05 were labeled as $Ni/Sn_{0.2}-SiO_2$ and $Ni/Sn_{0.05}-SiO_2$, respectively.

To investigate the effect of adding Sn as a nickel promoter, another catalyst was prepared by impregnating the $Ni-SiO_2$ catalyst with appropriate volume of 0.01 M solution of $SnCl_2$ in THF to yield Sn/Ni = 0.05. The sample was labeled $Sn_{0.05}/Ni-SiO_2$.

2.2. Catalyst Characterization. Specific surface areas and pore volumes of selected samples were determined from N_2 adsorption−desorption isotherms at −196 °C using a Micromeritics ASAP 2020 equipment, through the Brunauer−Emmett−Teller (BET) method in the standard pressure range of 0.05−0.3 P/P_0. Before the measurements, the samples were degassed at 250 °C for 2 h. By analysis of the desorption curve, using the BJH calculation method, the pore size distribution was also obtained.

https://doi.org/10.1021/acs.iecr.1c02193
Ind. Eng. Chem. Res. 2021, 60, 18684−18694

X-ray diffraction (XRD) analyses were carried out with a Bruker goniometer using Ni-filtered Cu Kα radiation. A proportional counter and a 0.05° step size in 2θ were used. The assignment of the crystalline phases was based on the Joint Committee on Powder Diffraction Standards (JCPDS) powder diffraction files (PDFs).[20] Crystallite sizes were estimated from diffraction line widths using the Scherrer equation.[21]

The X-ray photoelectron spectroscopy (XPS) analyses were carried out with a VG Microtech ESCA 3000 Multilab, equipped with a dual Mg/Al anode. As excitation source Al Kα radiation (1486.6 eV) was used. The sample powders were mounted on double-sided adhesive tape. The pressure in the analysis chamber was in the range of 10^{-8} Torr during data collection. The constant charging of the samples was eliminated by referencing all the energies to the C 1s binding energy set at 285.1 eV arising from adventitious carbon. Analyses of the peaks were carried out with the CasaXPS software. Atomic concentrations were calculated from peak intensity using the sensitivity factors provided by the software. The binding energy values are quoted with a precision of ±0.15 eV, and the atomic percentage are quoted with a precision of ±10%.

Hydrogen temperature-programmed reduction (TPR) measurements were carried out with a Micromeritics AutoChem 2950HP Automated Catalyst Characterization System, equipped with a thermal conductivity detector (TCD). About 0.1 g of sample was used for each measurement. The samples were pretreated with a mixture of 5 vol % O_2/He at 50 mL/min, heating (at 10 °C/min) to 400 °C, and holding at this temperature for 30 min. After lowering the temperature to room temperature, the gas mixture of 5 vol % H_2/Ar was introduced at 30 mL/min into the sample tube and was also used as a reference gas. During the analysis, the temperature was increased up to 1000 °C at a rate of 10 °C/min. The effluent gas was analyzed with a TCD.

The thermogravimetric analyses (TGA) of the samples after the catalytic reactions were carried out in air using the TGA 1 Star System of Mettler Toledo. About 10 mg of sample was heated from room temperature to 100 °C, left at this temperature for 1 h, and then heated to 1100 °C at the rate of 10 °C/min under air flowing at 30 mL/min.

2.3. Catalytic Activity. Methane dry reforming tests were carried out in a continuous-flow quartz reactor with an inner diameter of 12 mm. Powder samples of 40−60 mesh size were diluted 1:5 by weight with silicon carbide of the same mesh size of the catalyst. Prior the catalytic reaction, the catalysts were pretreated "in situ" under flowing O_2 (5 vol % in He, 50 mL/min) at 350 °C for 0.5 h. After cooling down to room temperature, the samples were reduced under flowing H_2 (5 vol % in He, 30 mL/min), and the temperature was increased to 550 or 750 °C with a 10 °C/min ramp and a holding time of 1 h. The feed gas, consisting of 15 vol % CH_4 + 15 vol % CO_2 in He, was led over the catalyst (100 mg) at a flow rate of 100 mL/min (STP), equivalent to a gas hourly space velocity (GHSV) of 60 000 mL g^{-1} h^{-1}. The activities were measured as a function of temperature from 450 to 800 °C with a heating rate of 10 °C/min, waiting 60 min for each 50 °C step. The samples were cooled to 650 °C and left at this temperature for 24 h of time on stream (TOS) for the stability test. The inlet and outlet gas compositions were analyzed by GC (Agilent 7890B) equipped with a DB-1 capillary column and a molecular sieve, in order to follow the evolution of all the species, CH_4, CO, CO_2, H_2, and O_2, using FID and TCD detectors. Water was condensed at the outlet of the reactor. CH_4 and CO_2 conversion, X_{CH_4}, X_{CO_2}, and hydrogen yield Y_{H_2} (%) were calculated as

$$X_{CH_4} = 100 \times ([CH_4]^{in} - [CH_4]^{out})/[CH_4]^{in}$$

$$X_{CO_2} = 100 \times ([CO_2]^{in} - [CO_2]^{out})/[CO_2]^{in}$$

$$Y_{H_2}(\%) = 100 \times [H_2]^{out}/2[CH_4{}^{in}]$$

3. RESULTS AND DISCUSSIONS

3.1. Catalytic Results. The DRM reaction test carried out on the $Sn_{4wt\%}-SiO_2$ support confirmed the inertness of the support and excluded any direct contribution of the tin to the catalytic activity of the supported nickel catalysts.[17] The catalytic results obtained with the various Ni samples at 650 °C are summarized in Table 1. In Figure 1, the CH_4 and CO_2 conversions, plotted as a function of temperature, along with the corresponding H_2/CO molecular ratio variations displayed in the insets, are shown for each of the four samples. With the exception of the $Ni/Sn_{0.05}-SiO_2$ sample, each panel of the figure compares the results obtained with the catalyst activated at two different reduction temperatures. In the case of the monometallic nickel catalyst, the CO_2 conversion and the CH_4 conversion run quite similarly. The CH_4 and the CO_2 conversions increase steadily with temperature in the range of 450−700 °C; thereafter, they increase slowly reaching the conversions of ∼95%, very close to the equilibrium value, with both the samples pre-reduced at 550 and 750 °C.[5] Similar behavior, with slightly superior conversions (see Table 1), is obtained with the tin-promoted Ni catalyst, $Sn_{0.05}/Ni-SiO_2$, with molar ratio Sn/Ni = 0.05. Moreover, compared to the sample reduced at 750 °C, the sample pre-reduced at 550 °C yields slightly higher CH_4 and CO_2 conversions. The catalyst, with the same formulation but prepared by supporting nickel over the Sn-promoted silica, $Ni/Sn_{0.05}-SiO_2$, exhibits significantly lower CH_4 conversion as compared to the CO_2 conversion. In the case of the $Ni/Sn_{0.2}-SiO_2$, with Sn/Ni = 0.2, the temperature of the H_2 pretreatment has a considerable effect. The starting CH_4 and CO_2 conversions at 400 °C are similar for both cases; however, with the increase of temperature, they start to diverge with a much larger CO_2 conversion as compared to the CH_4 conversion. Moreover, whereas with the 550 °C pre-reduced catalyst both conversions continue increasing with temperature, with the 750 °C pre-reduced catalyst at temperature above 600 °C, the increase of

Table 1. Catalytic Performance at 650 °C[a]

catalysts	conversion CH_4 (%)	conversion CO_2 (%)	H_2 yield (%)	H_2/CO
$Ni-SiO_{2\text{-}550}$	68.5 (2%)	73.6 (4%)	39.7	0.7
$Ni-SiO_{2\text{-}750}$	66.9(8%)	72.4(10%)	40.6	0.7
$Sn_{0.05}/Ni-SiO_{2\text{-}550}$	69.5(2%)	76.1 (5%)	41.1	0.7
$Sn_{0.05}/Ni-SiO_{2\text{-}750}$	66.9(5%)	73.7 (10%)	40.8	0.7
$Ni/Sn_{0.2}-SiO_{2\text{-}550}$	18.4 (8%)	26.1 (32%)	16.3	1
$Ni/Sn_{0.2}-SiO_{2\text{-}750}$	14.6 (24%)	19.9(33%)	17.1	0.9
$Ni/Sn_{0.05}-SiO_{2\text{-}550}$	61.3 (9%)	74 (5%)	42.4	0.7

[a]The deactivation after 24 h reaction is given in parentheses .

https://doi.org/10.1021/acs.iecr.1c02193
Ind. Eng. Chem. Res. 2021, 60, 18684−18694

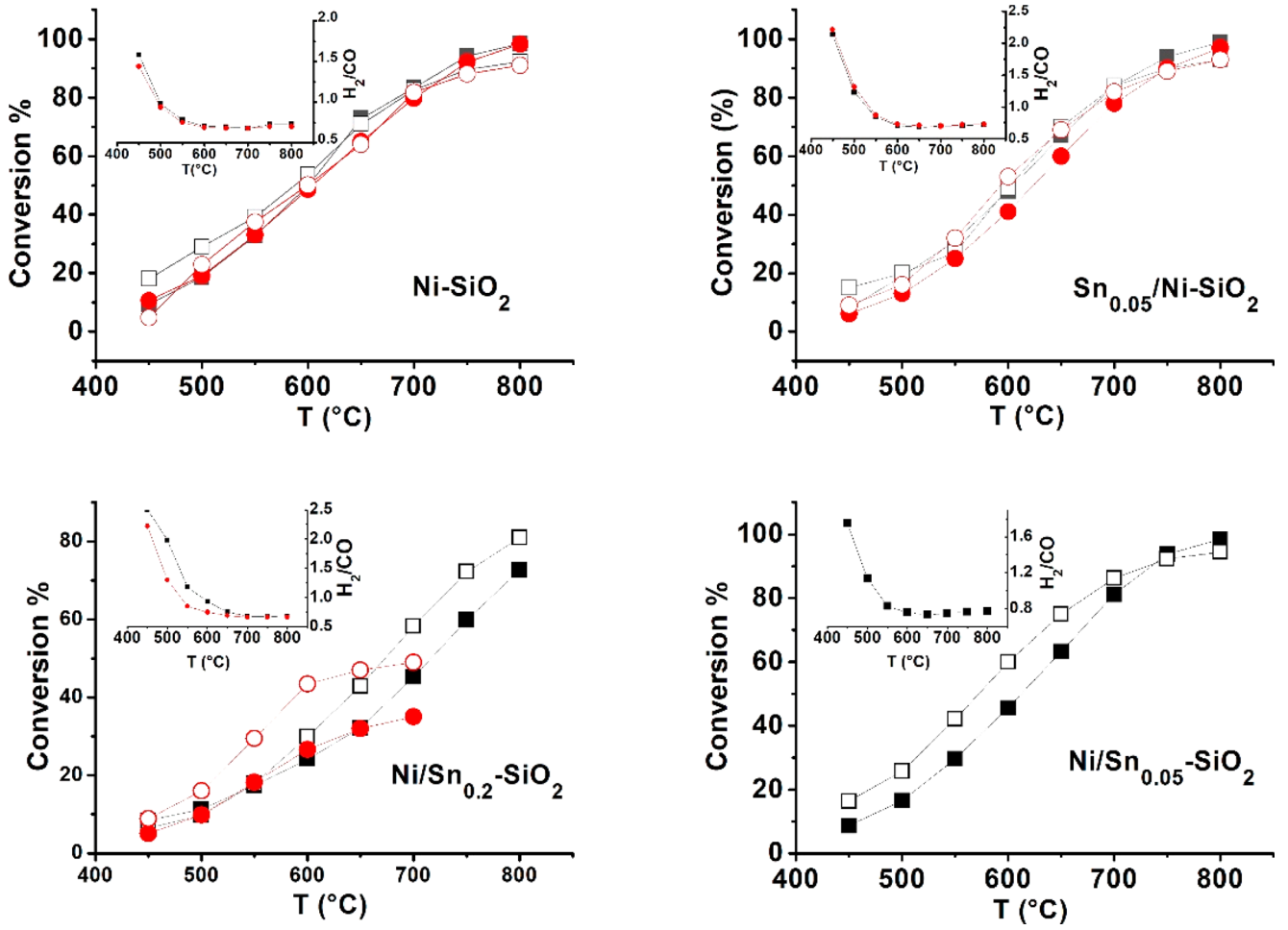

Figure 1. CH_4 (filled symbol) and CO_2 (empty symbol) conversion as a function of temperature for different samples pre-reduced at 750 °C (circle) and 550 °C (square). The plot in the inset refers to the corresponding H_2/CO molecular ratio variation.

conversion starts to decline. Overall, although the TPR analyses indicate a complete catalyst reduction at temperature above 750 °C, better catalytic performances are obtained with the samples activated at 550 °C rather than at 750 °C. As reported in the literature under similar experimental conditions, the occurrence of the reverse water gas shift reaction (RWGS) (the reverse of eq 2) was particularly significant between 400 and 800 °C and contributes to the increase of the CO_2 conversion as compared to the CH_4 conversion. At the same time, as observed with all the samples, the occurrence of RWGS explains the decrease of the H_2/CO molecular ratio with temperature.[22] The H_2/CO ratio of >2, obtained at the starting temperature of 400 °C may be caused by the occurrence of methane decomposition, producing an excess of hydrogen which then triggers the RWGS reaction. The larger H_2/CO ratio obtained for the bimetallic samples at the starting temperature, as shown in the inset of each panel, as compared to the monometallic nickel catalyst would suggest an enhancement of the methane decomposition reaction in the presence of tin.[23] As reported in the literature, the possible side reactions during DRM occur to an extent which is related not only to the experimental conditions such as pressure, CO_2/CH_4 ratio, and temperature but also to the catalyst properties such as the acidity−basicity of the support, metal−support interaction, and particle sizes.[1,2,4,11] The large variation of the H_2/CO ratio with temperature is related to the thermodynamic of all the possible reactions that may occur. Indeed, the exothermic reaction, such as the Boudouart reaction (eq 4), is favored at lower temperature and involves CO consumption, whereas the endothermic reactions such as the reaction of carbon with CO_2, (reverse Boudouart reaction) or the RWGS reaction would increase the CO yield at higher temperatures, therefore decreasing the H_2/CO molar ratio to 0.75.

The stability of the catalyst was checked by measuring methane conversion as a function of time over 24 h of reaction at 650 °C, a temperature of interest from the industrial point of view and for possible utilization of the biogas in an internal reforming SOFC.[3,23] It is important to note that the stability test followed the temperature gradient test, after cooling down to 650 °C. As seen in Figure 2 and in Table 1, although with some differences, all the studied catalysts do not deactivate substantially during the 24 h reaction at 650 °C. Better stability is observed with Ni−SiO_2 and $Sn_{0.05}$/Ni−SiO_2, deactivating only by 2% (as for the 550 °C pre-reduced samples). The Ni/$Sn_{0.05}$−SiO_2, prepared by supporting nickel over $Sn_{1wt\%}$−SiO_2, deactivates more rapidly, decreasing its methane conversion by 9% in 24 h. For the high tin-loaded catalyst, Ni/$Sn_{0.2}$−SiO_2, the deactivation of the catalyst, as observed in Figure 1, occurred quite rapidly as a function of temperature, and it was irreversible, since the starting conversions in Figure 2 are much lower than the corresponding values at 650 °C in Figure 1. In conclusion, with the exception of the high Sn content sample,

https://doi.org/10.1021/acs.iecr.1c02193
Ind. Eng. Chem. Res. 2021, 60, 18684−18694

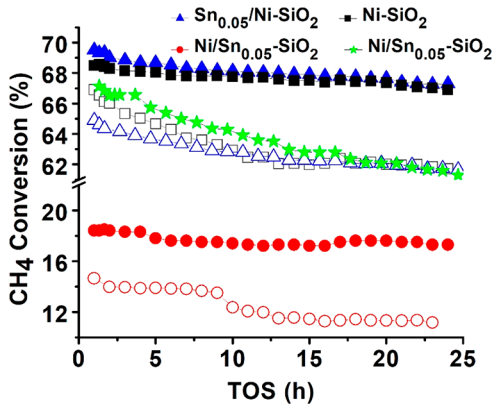

Figure 2. Stability test at 650 °C of the 550 °C (filled symbol) pre-reduced catalysts and 750 °C (empty symbol) pre-reduced catalysts.

the good stability generally observed for this series of catalysts, as compared to literature reported results, may be related to a stronger interaction between nickel particles and the silica support achieved during the microwave-assisted synthesis.[17,18] Moreover, a slightly superior stability of the catalysts pre-reduced at 550 °C is noticeable.

The amount of carbon built up over the samples at the end of the catalytic test was determined by TGA analyses. The profiles are given in Figure 3. All of them exhibit an initial increase of the weight, likely due to the reoxidation in air of the aged catalysts, followed by a weight loss due to the combustion of coke. Limited losses are observed, ranging from about 7 wt % for the monometallic nickel catalyst to about 2 wt % for the tin-doped samples. In particular, the catalysts made of nickel deposited over the tin-promoted silica, $Ni/Sn_{0.2}-SiO_2$ and the $Ni/Sn_{0.05}-SiO_2$, pre-reduced at 550 °C do not exhibit weight loss. The other catalysts, $Ni-SiO_2$ and the $Sn_{0.05}/Ni-SiO_2$, and the previous ones pre-reduced at 750 °C present some weight loss at temperature above 600 °C, attributed to amorphous or graphitic carbon combustion.[6,12]

Commenting on the catalytic results, summarized in Table 1, all the samples except the one with a Sn/Ni molar ratio of 0.2 exhibit good methane conversion and hydrogen yield as compared to the literature results.[17] In accord with recent literature on the effect of tin on nickel catalysts, a slightly superior activity is observed for the catalyst with a Sn/Ni molar ratio of 0.05, whereas much lower activity is obtained with the higher amount of Sn.[12] It is plausible that a large amount of tin hinders the accessibility of CH_4 and CO_2 on the surface of Ni therefore inhibiting their adsorption and dissociation, necessary steps for the outcome of the DRM reaction.[24] As noted before, it is particularly evident in Table 1 that the lower conversion for the $Ni/Sn_{0.2}-SiO_2$ sample, obtained during the stability test at 650 °C after the temperature gradient test, as compared to the corresponding value in Figure 1, was likely due to an irreversible sample deactivation. Moreover, by looking at the results of the long-term tests and those of the TGA, no direct correlation between the catalytic stability and the carbon formation is evinced. In fact, the monometallic $Ni-SiO_2$, with more carbon deposited during the reaction, maintains good methane conversion.

3.2. Characterization. *3.2.1. BET and XRD Analyses.* The list of catalysts with the corresponding BET specific surface areas, pore diameters, and pore volumes, along with crystallite sizes, is given in Table 2. The N_2 adsorption−desorption

Table 2. Surface Area (S_{BET}), Average Pore Diameter (d_p), and Pore Volume V_p of Supports and Catalysts[a]

samples	S_{BET} ($m^2\ g^{-1}$)	d_p (nm)	V_p (cm^3/g)	d_{NiO} (nm)	d_{Ni} (nm)	d_{SnO_2} (nm)
SiO_2	657	4.1	0.85			
$Sn_{4wt\%}-SiO_2$	508	4.7	0.69			2.5
$Sn_{1wt\%}-SiO_2$	646	4.5	0.92			n.d.
$Ni-SiO_2$	476	4.7	0.58	2.7	2.9[b] 4.6[b]	
$Ni/Sn_{0.2}-SiO_2$	455	5.2	0.58	2.3	2.9[b] 4.2[c]	2.4
$Sn_{0.05}/Ni-SiO_2$	518	4.7	0.59	2.0	2.6[b] 3.9[c]	n.d.
$Ni/Sn_{0.05}-SiO_2$	599	4.8	0.82	3.5	4.0[b]	n.d.

[a]The NiO, Ni, and SnO_2 crystallite sizes, as determined from Scherrer analyses of XRD peaks are also listed. [b]Ni or Ni_xSn_y particle sizes after DRM with pre-reduction at 550 °C; [c]Ni or Ni_xSn_y particle sizes after DRM with pre-reduction at 750 °C.

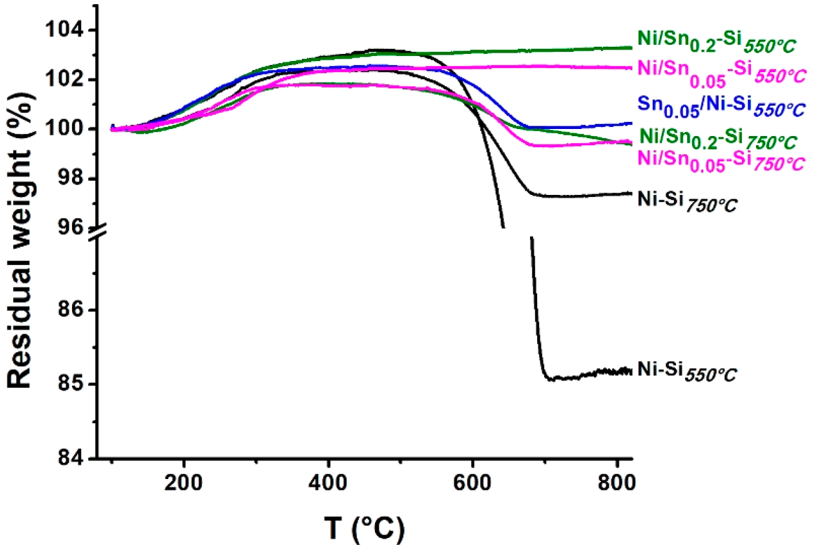

Figure 3. TGA profiles of catalysts after DRM reaction with different pre-reduction temperatures (due to space reason Si replaces SiO_2).

https://doi.org/10.1021/acs.iecr.1c02193
Ind. Eng. Chem. Res. 2021, 60, 18684−18694

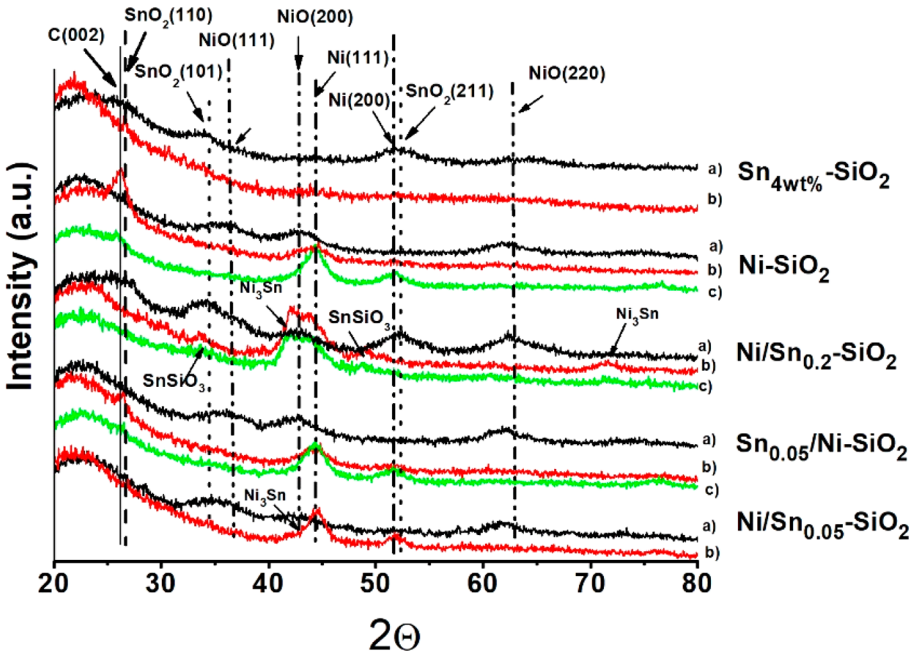

Figure 4. XRD patterns of the different catalysts and tin doped support: (a) before, (b) after catalytic test with H_2 pre-reduction at 550 °C, and (c) after catalytic test with H_2 pre-reduction at 750 °C.

isotherms along with the pore sizes distribution are plotted in Figure S1. For comparison reasons, the data relative to the supports SiO_2 and $Sn_{4wt\%}-SiO_2$ are also reported. According to the IUPAC classification, the isotherms are of type IV, characteristic of mesoporous materials, with clear hysteresis loops of H1 type.[25] The second hysteresis observed at a higher relative pressure, $P/P_0 > 0.8$, indicates textural pores resulting from the packing of small particles.[26] As observed in Table 2, adding tin and subsequently nickel causes a gradual decrease of surface area with an increase of the average pore sizes.

The X-ray diffraction patterns of the samples, as-calcined and after the DRM reaction, recorded for the 550 and 750 °C pre-reduced catalysts are shown in Figure 4. For comparison reason the pattern of the $Sn_{4wt\%}-SiO_2$ support is also reported. The pattern of tin doped silica exhibits the broad band at $2\theta \sim 22°$ typical of amorphous silica and additional peaks at $2\theta \sim 34$ and ~52° attributable to the reflection (101) and (211) of the tetragonal SnO_2 (PDF no. 04−003−0649, JCPDS). It is worth noting how the tin oxide reflections disappear from the pattern of the sample exposed to the DRM conditions, likely due to a dispersion of tin into the silica bulk. With respect to the calcined samples, the diffractogram of $Ni-SiO_2$ contains broad peaks attributed to the (111), (200), and (220) reflections of cubic NiO crystallites (PDF no. 04−002−4405, JCPDS). Peaks belonging to SnO_2 and NiO are present in the diffractogram of $Ni/Sn_{0.2}-SiO_2$, whereas only reflections attributable to NiO are present in the diffractogram of the $Ni/Sn_{0.05}-SiO_2$ and $Sn_{0.05}/Ni-SiO_2$ samples. An estimate of the crystallite sizes, carried out by the Scherrer analyses of the (211) reflection and of the (220) reflections of SnO_2 and NiO, respectively, are included in Table 2. Quite small and comparable sizes are obtained for SnO_2 and NiO crystallites respectively in mono- and bimetallic samples. As reported in previous studies, such small sizes are a prerogative of the microwave-assisted preparation procedure, as compared to the traditional incipient wetness impregnation, which yields larger crystallite sizes.[27,28] The diffractograms of the spent catalysts reflect the modification sustained by the samples during the catalytic test. In the pattern of $Ni-SiO_2$ after DRM on the sample pre-reduced at 550 °C, along with a diffraction peak at $2\theta = 44.5°$ attributed to the (111) reflection of the metallic nickel (PDF no. 04−010−6148, JCPDS), a peak at $2\theta = 26°$ attributed to hexagonal graphite is present. On the basis of the (111) reflection, a nickel particle size of 2.9 nm was estimated. As suggested by the asymmetry of the peak, the low-angle tail of the broad (111) reflection partially overlaps with the (200) reflection at $2\theta = 43.3°$ of some unreduced NiO. After DRM on the Ni/SiO_2 pre-reduced at 750 °C, the reflections of the metallic nickel, (111) at $2\theta = 44.5°$ and (200) at $2\theta = 51.8°$, become sharper, corresponding to a larger Ni particle size of about 4.6 nm. On the contrary, the graphite peak seems weakened, in accord with the smaller weight loss observed in the TGA profiles of the corresponding spent catalyst in Figure 3. The diffractograms of the spent $Ni/Sn_{0.2}-SiO_2$ catalyst exhibit a complex feature in the region of the most intense metallic nickel reflection Ni (111). The region contains characteristic peaks of Ni_3Sn alloy (PDF no. 00−063−0098, JCPDS) and metallic Ni.[28] From the fitting of the two peak components and applying the Scherrer equation, particle sizes of 2.9 and 4.2 nm for both metallic components were estimated for the spent samples pre-reduced at 550 and 750 °C, respectively. Small reflections at $2\theta = 34$ and 48° are attributed to the tin silicate $SnSiO_3$ (PDF no. 00−020−1295, JCPDS). The XRD patterns of the spent $Sn_{0.05}/Ni-SiO_2$ and $Ni/Sn_{0.05}-SiO_2$ contain reflections attributable to Ni(111) and Ni (220) with low-angle asymmetry attributed to Ni_xSn_y alloy contribution. The diffractogram of the spent $Sn_{0.05}/Ni-SiO_2$ pre-reduced at 550 °C also contains a small peak at $2\theta = 26°$, attributable to graphitic carbon. Particle sizes of 2.6 and 3.9 nm for the spent $Sn_{0.05}/Ni-SiO_2$ catalysts pre-reduced at 550 and 750 °C, respectively, were estimated. Ni crystallite size of 4.0 nm was obtained for the spent $Ni/Sn_{0.05}-SiO_2$ activated at 550 °C. Differences in particle sizes, as estimated from the XRD patterns of the spent samples can account for differences in

https://doi.org/10.1021/acs.iecr.1c02193
Ind. Eng. Chem. Res. 2021, 60, 18684−18694

catalytic performance and in carbon formation. In particular, the bimetallic catalysts pre-reduced at 550 °C, characterized by a better activity, present smaller Ni particles after reaction.

3.2.2. TPR Analyses. In order to investigate the redox behavior of the catalysts, particularly the effect of tin on nickel reducibility, TPR analyses were carried out. For comparison reason, the high loaded $Sn_{4wt\%}-SiO_2$ support was analyzed as well. The hydrogen reduction profiles are shown in Figure 5.

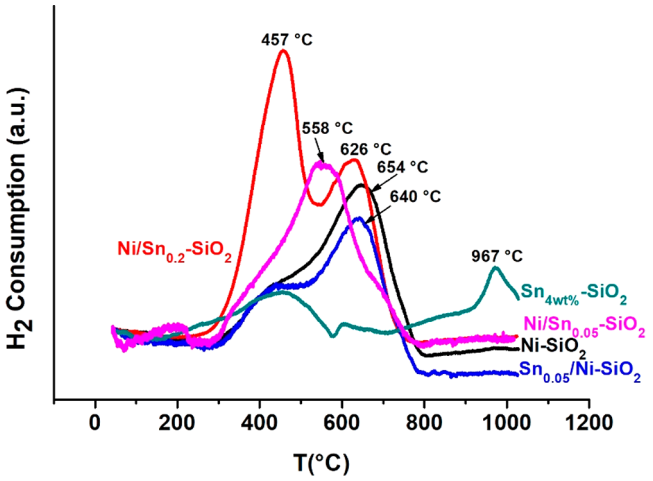

Figure 5. TPR of supported catalysts and tin-containing support.

The results of the peak integration in terms of maximum temperature peak position (T_{max}) and corresponding H_2 volume (V_{H_2}) consumption are listed in Table 3. The TPR profile of nickel supported on bare silica contains a main peak at 654 °C and a shoulder at around 440 °C. The high-temperature peak corresponds to the reduction of small NiO particles with strong $Si-O^{\delta}-Ni^{\delta+}$ interaction hard to reduce.[7,8] Larger size NiO crystallites with a lower degree of interaction with the silica support gave rise to the broad shoulder at lower temperature. The total hydrogen consumption, consistent with 9 wt % nickel instead of the nominal 10 wt %, accounts for the formation of hard to reduce nickel silicate inhibiting the complete NiO reduction.[22] The TPR profile of the high loaded $Sn_{4wt\%}-SiO_2$ support is characterized by a broad feature peaked at around 440 °C attributed to the reduction of tin dioxide SnO_2, and a sharper peak at 970 °C attributable to a difficult to reduce tin silicate. The SnO_2 reduction temperature of 440 °C is much lower than the reduction temperature of 670 °C reported in the literature for Sn-doped SiO_2.[28] A reciprocal effect between nickel and tin is observed in the TPR profile of the catalyst $Ni/Sn_{0.2}-SiO_2$, characterized by two strong peaks, one at 457 °C and the other at 626 °C. It is reasonable, on the basis of the reduction temperature observed for the tin-doped support, to attribute the stronger low-temperature peak to a combination of nickel and tin reduction more closely interacting together and the high-temperature peak to the reduction of "free" nickel oxide. Subtracting the hydrogen consumption attributable to the reduction of SnO_2 as derived from the TPR of the $Sn_{4wt\%}-SiO_2$ sample, it was possible to estimate that about 5 wt % nickel was in close contact with Sn and another 5 wt % was "free" NiO. The presence of tin increased the nickel reducibility, by decreasing its reduction temperature, and the presence of nickel increased the tin reducibility, by downshifting the 970 °C peak, making easier the formation of a Ni_xSn_y alloy, as detected by XRD.[15,28] The sample $Ni/Sn_{0.05}-SiO$ exhibits a TPR profile with a large peak centered at 558 °C, corresponding to the reduction of mixed SnO_2-NiO oxides in close contact with each other, and broad shoulders on the left and on the right side of the main peak, corresponding to isolated tin and nickel oxides. The TPR profile of $Sn_{0.05}/Ni-SiO_2$ is rather similar to the profile of the unpromoted nickel catalyst. The only difference is the little extra hydrogen consumption for the low-temperature peak attributed to the reduction of tin oxide. According to the TPR results, focusing on the two samples having the same composition, the addition of tin to the already prepared $Ni-SiO_2$ catalyst has a modest effect on the nickel reducibility, maintaining a similar TPR profile. On the contrary, adding nickel to the Sn-doped support seems to produce a chemical species which reduces at an intermediate temperature between the SnO_2 and the NiO reduction temperature.

Table 3. T_{max} and Corresponding H_2 Volume Consumption (V_{H_2}) Obtained from TPR Analyses

	T_{max} (°C)		V_{H_2} (mL/g_{cat})	
sample	first peak	second peak	first peak	second peak
$Sn_{4wt\%}-SiO_2$	440	967	7	5
$Ni-SiO_2$	450	640	9	19
$Ni/Sn_{0.2}-SiO_2$	457	626	30	18
$Ni/Sn_{0.05}-SiO_2$		558		33
$Sn_{0.05}/Ni-SiO_2$	521	642	10	20

3.2.3. XPS Analyses. XPS measurements of the fresh (calcined) and spent catalysts were carried out in order to investigate the distribution and the chemical state of each catalyst component and the modification occurring upon reactions. The Ni 2p spectra of the catalysts as fresh and after the DRM reaction with different hydrogen pretreatment temperatures are given In Figure 6. The results in terms of binding energies and atomic ratios are summarized in Tables 4 and 5 for the fresh and spent samples respectively. The fresh samples are characterized by Ni 2p spectra typical of Ni^{2+} with Ni $2p_{3/2}$ binding energy of 855.7 ± 0.2 eV and prominent shake-up peaks.[29] The presence of tin does not modify the Ni oxidation state of the calcined samples. After the DRM reaction, the Ni 2p spectra contain components attributed to metallic Ni along with oxidized nickel components. It is worth noting the difference in the binding energy attributed to metallic nickel, between the value of 852.6 ± 0.1 eV for the undoped nickel catalyst and the value around 852.0 ± 0.2 eV for the Sn-doped samples. In accord with literature, such a shift is indicative of an electron transfer from Sn to Ni, as in an alloy phase Ni_xSn, which reflects an increase of the electron density on the nickel atoms.[28] In spite of precautions to limit exposure of the spent samples to air, some reoxidation likely occurred in the spent samples after being removed from the reactor and before being introduced into the XPS vacuum environment. For this reason, a precise correlation between percentages of reduced nickel and structural, chemical, and compositional properties or different reaction conditions could not be claimed. However, it appears that regardless of the pre-reduction temperature the Ni 2p spectra of spent $Sn_{0.05}/Ni-SiO_2$ samples present a large fraction of reduced nickel, whereas the spectra of the samples prepared by adding nickel to the Sn-doped silica exhibit a smaller fraction of metallic nickel after DRM reaction. On the basis of TPR profiles,

https://doi.org/10.1021/acs.iecr.1c02193
Ind. Eng. Chem. Res. 2021, 60, 18684−18694

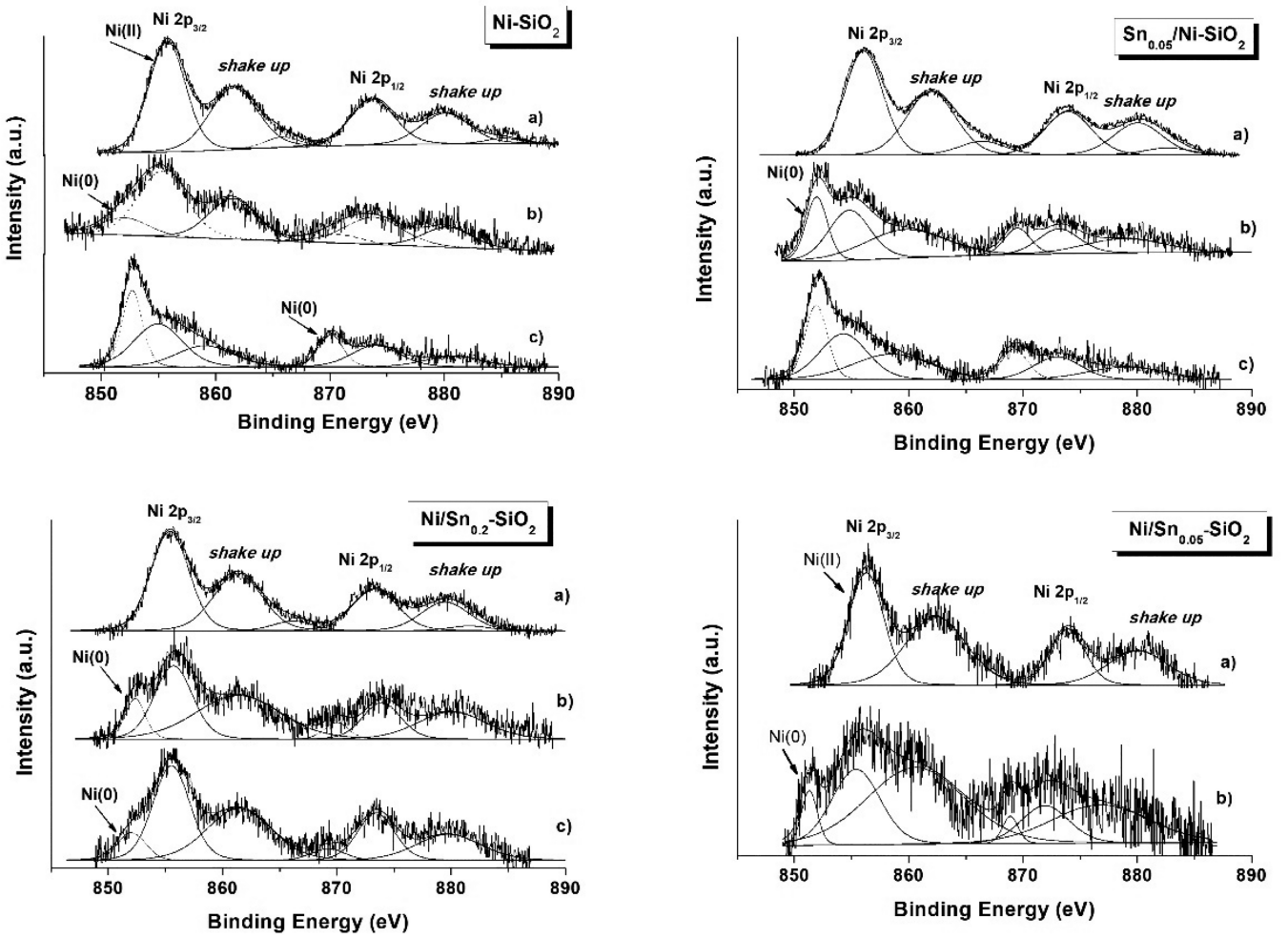

Figure 6. Ni 2p XP spectra of different catalysts: (a) fresh, (b) after reaction with H_2 pre-reduction at 550 °C, and (c) after reaction with H_2 pre-reduction at 750 °C.

Table 4. Binding Energies (eV) of the Main Element Photoelectron Peaks and XPS-Derived Atomic Ratios of Calcined Samples

samples	Sn $3d_{5/2}$[a]	Ni $2p_{3/2}$	Sn/Si[b]	Ni/Si	Sn/Ni
$Sn_{4wt\%}-SiO_2$	487.7		0.01 (0.02)		
$Sn_{1wt\%}-SiO_2$	487.3(79) 485.4(21)		0.004 (0.006)		
$Ni-SiO_2$		855.7		0.24(0.11)	
$Sn_{0.05}/Ni-SiO_2$	487.6	855.9	0.009 (0.006)	0.18(0.13)	0.05(0.05)
$Ni/Sn_{0.05}-SiO_2$	487.7(68) 486.2(32)	855.9	0.005 (0.006)	0.05(0.13)	0.11(0.05)
$Ni/Sn_{0.2}-SiO_2$	487.6	855.6	0.01 (0.02)	0.19 (0.12)	0.07 (0.18)

[a]The values in parentheses refer to the relative atomic percentage of each chemical components [b]The values in parentheses refer to the nominal value.

similar extent of reduction is expected for all the catalysts after the H_2 activation at the temperatures of 550 and 750 °C. Therefore, the difference in the XPS-derived percentage of Ni reduction may be attributed to a different sensitivity to the air exposure or, more likely, to different structural modifications during the reaction. The Sn 3d spectra of the support $Sn_{4wt\%}-SiO_2$ and of the catalysts are shown in Figure 7. The Sn 3d spectra of the calcined samples are characterized by the two spin−orbit components, Sn $3d_{5/2}$ and Sn $3d_{3/2}$, 8.5 eV apart. The position of the Sn $3d_{5/2}$ peak at 487.6 ± 0.1 eV is typical of a highly oxidized Sn^{4+}.[5] The calcined $Ni/Sn_{0.05}-SiO_2$ exhibits an additional Sn $3d_{5/2}$ component at 486.2 eV attributed to a less oxidized Sn^{2+}, probably arising from the species $SnSiO_3$, detected by XRD after the reaction but likely being formed during the catalyst calcination. However, a similar value of the Sn $3d_{5/2}$ component, obtained for a Sn-doped Ni catalyst supported on alumina, was attributed to an intermetallic compound on the surface of the Ni particles.[30,31] After being exposed to the DRM test conditions, including pre-reduction at 550 °C, the Sn $3d_{5/2}$ component of the $Sn_{4wt\%}-SiO_2$ support shifts by only 0.4 eV toward a lower binding energy. More complex spectra are obtained for the spent

https://doi.org/10.1021/acs.iecr.1c02193
Ind. Eng. Chem. Res. 2021, 60, 18684−18694

Table 5. Sn $3d_{5/2}$ and Ni $2p_{3/2}$ Binding Energy (eV) and Atomic Ratios of Aged Samples after the Dry Reforming Test Performed on Samples Reduced at 550 and 750 °C[a]

	Sn $3d_{5/2}$		Ni $2p_{3/2}$		Sn/Si		Ni/Si		Sn/Ni	
aged samples	550 °C	750 °C	550 °C	750 °C	550 °C	750 °C	550 °C	750 °C	550 °C	750 °C
$Sn_{4wt\%}-SiO_2$	487.3				0.09					
Ni/SiO_2			855.6(84)	855.7(68)			0.1	0.09		
			852.7(16)	852.6(32)						
$Sn_{0.05}/Ni-SiO_2$	486.5	486.4	855.2(76)	855.3(70)	0.006	0.007	0.10	0.11	0.06	0.06
			852.0(24)	852.0(30)						
$Ni/Sn_{0.05}-SiO_2$	487.0(33)	n.a.[b]	855.2(87)	n.a.[b]	0.005	n.a.[b]	0.03	n.a.[b]	0.15	n.a.[b]
	485.8(67)		851.8(13)							
$Ni/Sn_{0.2}-SiO_2$	487.2(80)	487.1(70)	855.6(89)	855.4(88)	0.03	0.04	0.12	0.12	0.25	0.33
	485.4(20)	485.5(30)	852.2(11)	852.0(12)						

[a]The relative amount of each element component is given in parentheses. [b]n.a.: not available

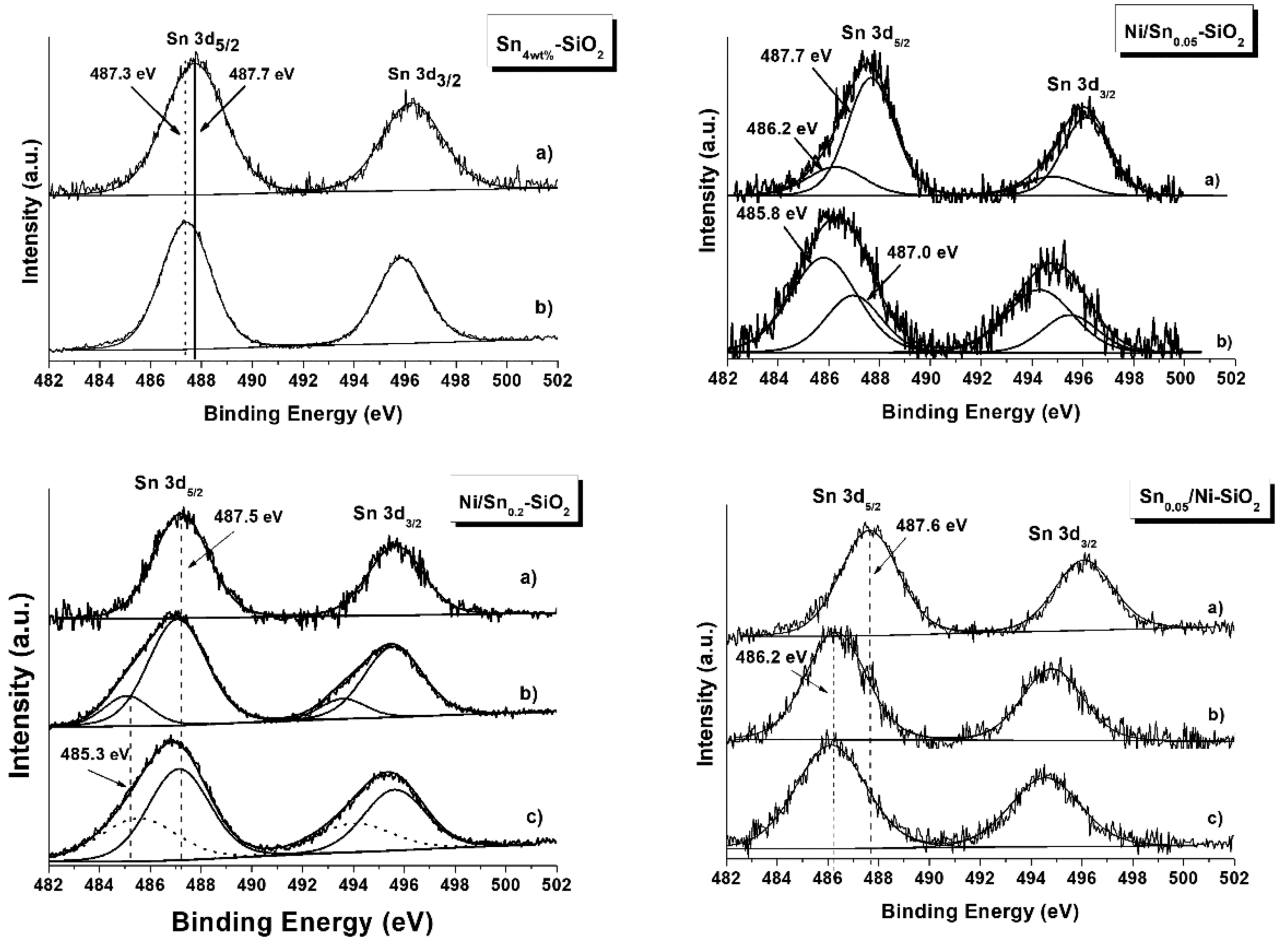

Figure 7. Sn 3d XP spectra of support and catalysts: (a) as calcined, (b) after reaction with H_2 pre-reduction at 550 °C, and (c) after reaction with H_2 pre-reduction at 750 °C.

catalysts. The Sn 3d spectra of the $Ni/Sn_{0.2}-SiO_2$ was fitted with two spin−orbit doublet components. One component, characterized by a Sn $3d_{5/2}$ peak at 487.3 eV, is attributed to oxidized tin. The other component characterized by a Sn $3d_{5/2}$ peak at 485.3 eV, due to reduced Sn, indicates an easier reduction of tin in the presence of nickel. The binding energy value, higher than the value commonly reported for metallic tin, is in accord with the energy shift in the opposite direction, observed for the Ni $2p_{3/2}$ and attributed to the electron transfer from tin to nickel upon alloy formation.[28] Analogously, the Sn 3d spectrum of the $Ni/Sn_{0.05}-SiO_2$ was also fitted with two doublet components. In the case of the spent catalyst $Sn_{0.05}/Ni-SiO_2$, only one spin−orbit doublet was fitted, with the Sn $3d_{5/2}$ peak centered at 486.2 eV. The value is typical of Sn^{2+}. It is worth noting how the evolution of the Ni 2p and the Sn 3d spectra during the reaction are related to each other. Indeed, when Sn is added over $Ni-SiO_2$, as in $Sn_{0.05}/Ni-SiO_2$, a Sn $3d_{5/2}$ peak typical of oxidized Sn^{2+} is registered in the sample after reaction, with more of the Ni 2p maintained as metallic Ni. The opposite is observed with the samples prepared with Ni added to the Sn-doped silica. Indeed, in $Ni/Sn_{0.05}-SiO_2$ an additional Sn $3d_{5/2}$ component typical of

https://doi.org/10.1021/acs.iecr.1c02193
Ind. Eng. Chem. Res. 2021, 60, 18684−18694

metallic Sn is registered, and less metallic Ni is found. A sort of reciprocal protection of the reduction state is made by the element being added as last one.

Some further information on the catalyst surface compositional changes are obtained from the intensity ratio variations summarized in Tables 4 and 5. The support, $Sn_{4wt\%}-SiO_2$, as suggested by the Sn/Si atomic ratio, has a relative surface concentration of Sn lower than the bulk concentration. Such a result would be in accord with a tendency of tin to diffuse inside the silica matrix under the sample preparation conditions, including the high-temperature calcinations, and aggregate as SnO_2, in accord with XRD results. A better Sn surface dispersion is observed with the lower tin loading sample, $Sn_{1wt\%}-SiO_2$. Upon exposure to the DRM environment, including pre-reduction at 550 °C, the Sn/Si atomic ratio increases substantially due to an outward tin diffusion, driven by the reducing reaction atmosphere. The catalysts prepared by adding Ni to the Sn-doped silica, in the calcined state, have also less tin at the surface as compared to the nominal concentration, probably covered by the added nickel. In the case of $Sn_{0.05}/Ni-SiO_2$, prepared by adding tin to the $Ni-SiO_2$ sample, the surface atomic ratio Sn/Ni is close to the nominal value, suggesting a more uniform distribution of tin within the nickel oxide particle. As observed in Table 5, upon DRM tests, Sn segregates at the catalyst surface, with a net increase of the Sn/Ni atomic ratio, to a large extent in $Ni/Sn_{0.2}-SiO_2$. The tin segregates partially as an alloy and partially as oxidized tin, as derived from the binding energies and in accord with the XRD detection of the Ni_3Sn alloy and $SnSiO_3$ silicate. A better surface compositional stability is observed with $Sn_{0.05}/Ni-SiO_2$, which in the spent state maintains the same Sn/Ni atomic ratio as the calcined state. A more effective Ni−Sn interaction, achieved during the preparation procedure, could likely explain such behavior. From purely statistic consideration, the probability for a few atoms of Sn to impact the more abundant Ni atoms already deposited on silica is superior with respect to the case of more abundant atoms of nickel impacting fewer atoms of tin. In this case, most of the nickel will deposit over the silica rather than over the tin.

In conclusion, upon reaction, the sample with a low amount of tin, prepared by adding tin after the nickel, maintains its original surface composition, and according to the binding energy values of Sn $3d_{5/2}$ and Ni $2p_{3/2}$, it contains more metallic tin alloyed with nickel. The presence of the alloy would inhibit nickel particle growth and would contribute to a better catalytic stability. The amount of alloy species is likely too low to be visible in the XRD pattern. The sample with the same composition but prepared by adding nickel to the tin-doped silica exhibits tin segregation at the surface driven by the reaction, explaining the easier deactivation of the catalyst during DRM. The sample with a larger amount of tin, analogously prepared, upon catalytic test forms XRD-detectable crystallites of Ni_3Sn, along with "free" tin having a strong tendency to segregate to the surface, which is then easily reoxidized to Sn^{2+} upon a short exposure to air. The poor activity of the catalyst is explained by the Ni active sites being covered by Sn.

4. CONCLUSION

A 10 wt % Ni catalyst supported on high-surface-area silica, prepared via a microwave-assisted precipitation method exhibited good catalytic performance in DRM with carbon dioxide, achieving 70% methane conversion at 650 °C and close to 95% conversion at 800 °C. During 24 h on stream, it was deactivated by only 2% at 650 °C with some carbon deposition on the catalyst surface. Doping silica with 4 wt % Sn, corresponding to a Sn/Ni molar ratio of 0.2, produces much less active catalyst in terms of methane and CO_2 conversion, in spite of the low coke formation. Decreasing the amount of tin to 1 wt %, corresponding to a Sn/Ni ratio of 0.05, produces an active catalyst which, however, deactivates quicker with respect to the monometallic nickel. Sintering of the Ni particles in the absence of carbon formation is likely the reason for the catalyst deactivation. Modifying the preparation procedure by changing the sequence of the element addition, i.e., adding tin to the monometallic nickel catalyst, maintaining the Sn/Ni ratio at 0.05, produces a slight increase of the catalytic activity with good catalyst stability, along with a reduced coke formation with respect to the undoped Ni catalyst. According to the structural characterization, the addition of a small quantity of tin is favorable because of electronic and geometric effects associated with a Ni_xSn_y alloy. Most importantly, a beneficial effect of tin is observed when it is added as metal promoter rather than as a support modifier.

■ ASSOCIATED CONTENT

Supporting Information

The Supporting Information is available free of charge at https://pubs.acs.org/doi/10.1021/acs.iecr.1c02193.

N_2 adsorption/desorption isotherms and pore size distribution curves of SiO_2-supported catalysts and support (PDF)

■ AUTHOR INFORMATION

Corresponding Authors

Anna Maria Venezia − *ISMN-CNR, 90146 Palermo, Italy;* orcid.org/0000-0001-7197-875X; Email: annamaria.venezia@cnr.it

Valeria La Parola − *ISMN-CNR, 90146 Palermo, Italy;* orcid.org/0000-0001-7695-6031; Email: valeria.laparola@cnr.it

Authors

Giuseppe Pantaleo − *ISMN-CNR, 90146 Palermo, Italy;* orcid.org/0000-0002-2474-8481

Maria Luisa Testa − *ISMN-CNR, 90146 Palermo, Italy;* orcid.org/0000-0003-1898-6608

Complete contact information is available at: https://pubs.acs.org/10.1021/acs.iecr.1c02193

Notes

The authors declare no competing financial interest.

■ ACKNOWLEDGMENTS

The bilateral project between the CNR and the Bulgarian Academy of Science (BAS) is kindly acknowledged.

■ REFERENCES

(1) Seo, H. O. Recent Scientific Progress on Developing Supported Ni catalysts for Dry (CO2) Reforming of Methane. *Catalysts* **2018**, *8*, 110.

(2) Aramouni, N. A. K.; Touma, J. G.; Tarboush, B. A.; Zeaiter, J.; Ahmad, M. N. Catalyst design for dry reforming of methane: Analysis Reviews. *Renewable Sustainable Energy Rev.* **2018**, *82*, 2570−2583.

(3) Cai, X.; Hu, Y. H. Advances in catalytic conversion of methane and carbon dioxide to highly valuable products. *Energy Sci. Eng.* **2019**, *7*, 4−29.
(4) Djinović, P.; Batista, J.; Pintar, A. Efficient catalytic abatement of greenhouse gases: methane reforming with CO_2 using a novel and thermally stable Rh-CeO_2 catalyst. *Int. J. Hydrogen Energy* **2012**, *37*, 2699−2707.
(5) Nikoo, M. K.; Amin, N. A. S. Thermodynamic analysis of carbon dioxide reforming in view of solid carbon formation. *Fuel Process. Technol.* **2011**, *92*, 678−691.
(6) Liu, J.; Peng, H.; Liu, W.; Xu, X.; Wang, X.; Li, C.; Zhou, W.; Yuan, P.; Chen, X.; Zhang, W.; Zhan, H. Tin Modification on Ni/Al_2O_3: Designing Potent Coke-Resistant Catalysts for the Dry Reforming of methane. *ChemCatChem* **2014**, *6*, 2095−2104.
(7) Boldrin, P.; Ruiz-Trejo, E.; Mermelstein, J.; Bermudez Menendez, J. M.; Ramırez Reina, T.; Brandon, N. P. Strategies for carbon and sulfur tolerant solid oxide fuel cell materials incorporating lessons for heterogeneous catalysis. *Chem. Rev.* **2016**, *116* (22), 13633−13684.
(8) Bengaard, H. S.; Norskov, J. K.; Sehested, J.; Clausen, B. S.; Nielsen, L. P.; Molenbroek, M.; Rostrup-Nielsen, J. R. Steam Reforming and Graphite Formation on Ni Catalysts. *J. Catal.* **2002**, *209*, 365−384.
(9) Abild-Pedersen, F.; Lytken, O.; Engbaek, J.; Nielsen, G.; Chorkendorff, I.; Norskov, J. K. Methane Activation on Ni(111): Effect of Poisons and Step Defects. *Surf. Sci.* **2005**, *590*, 127−137.
(10) Hu, Y. H.; Ruckenstein, E. Catalytic conversion of methane to synthesis gas by partial oxidation and CO_2 reforming. *Adv. Catal.* **2004**, *48*, 297−345.
(11) Arora, S.; Prasad, R. An overview on dry reforming of methane: strategies to reduce carbonaceous deactivation of catalysts. *RSC Adv.* **2016**, *6*, 108668−108688.
(12) Guharoy, U.; Le Saché, E.; Cai, Q.; Reina, T. R.; Gu, S. Understanding the role of Ni-Sn interaction to design highly effective CO_2 conversion catalysts for dry reforming of methane. *J. CO2 Util.* **2018**, *27*, 1−10.
(13) Saadi, S.; Hinnemann, B.; Helveg, S.; Appel, C. C.; Abild-Pedersen, F.; Nørskov, J. K. First- principles investigations of the Ni3Sn alloy at steam reforming conditions. *Surf. Sci.* **2009**, *603*, 762−770.
(14) Ai, M. The oxidation activity and acid-base properties of SnO_2-based binary catalysts: I. The SnO_2-V_2O_5 system. *J. Catal.* **1975**, *40*, 318−326.
(15) Nikolla, E.; Schwank, J.; Linic, S. Promotion of the long − term stability of reforming Ni catalysts by surface alloying. *J. Catal.* **2007**, *250*, 85−93.
(16) Baudouin, D.; Candy, J. P.; Rodemerck, U.; Krumeich, F.; Veyre, L.; Webb, P. B.; Thieuleux, C.; Coperet, C. Preparation of Sn-doped 2−3nm Ni nanoparticles supported on SiO_2 via surface organometallic chemistry for low temperature dry reforming catalyst: the effect of tin doping on activity, selectivity and stability. *Catal. Today* **2014**, *235*, 237−244.
(17) Stroud, T.; Smith, T. J.; Le Saché, E.; Santos, J. L.; Centeno, M. A.; Arellano-Garcia, H.; Odriozola, J. A.; Reina, T. R. Chemical CO_2 recycling via dry and bi reforming of methane using Ni-Sn/Al_2O_3 and Ni-Sn/CeO_2-Al_2O_3 catalysts. *Appl. Catal., B* **2018**, *224*, 125−135.
(18) Emamdoust, A.; La Parola, V.; Pantaleo, G.; Testa, M. L.; Farjami Shayesteh, S.; Venezia, A. M. SiO_2 Supported Ni and Ni-Ce Catalysts for Partial Oxidation of Methane. *J. Energy Chem.* **2020**, *47*, 1−9.
(19) Polychronopoulou, K.; Zedan, A. F.; AlKetbi, M.; Stephen, S.; Ather, M.; Katsiotis, M. S.; Arvanitidis, J.; Christofilos, D.; Isakovic, A. F.; AlHassan, S. Tailoring the efficiency of an active catalyst for CO abatement through oxidation reaction: The case study of samarium-doped ceria. *J. Environ. Chem. Eng.* **2018**, *6*, 266−280.
(20) *Inorganic Crystal Structure Database (ICSD)*; FIZ Karlsruhe GmbH: Eggenstein-Leopoldshafen, Germany, 2014.
(21) Klug, H. P.; Alexander, L. E. *X-ray Diffraction Procedures for Polycrystalline and Amorphous Materials*, 2nd ed.; John Wiley and Sons: New York, 1974.
(22) Ali, S.; Khader, M. M.; Almarri, M.; Abdelmoneim, A. G. Ni-Based Catalysts for the dry reforming of methane. *Catal. Today* **2020**, *343*, 26−37.
(23) Le Sachè, E.; Johnson, S.; Pastor-Perez, L.; Amini Horri, B.; Reina, T. R. Biogas Upgrading Via Dry Reforming Over a Ni-Sn/CeO_2-Al_2O_3 Catalyst: influence of Biogas Source. *Energies* **2019**, *12*, 1007.
(24) Erdohelyi, A.; Cserényi, J.; Papp, E.; Solymosi, F. Catalytic reaction of methane with carbon dioxide over supported palladium. *Appl. Catal., A* **1994**, *108*, 205−219.
(25) Thommes, M.; Kaneko, K.; Neimark, A. V.; Olivier, J. P.; Rodriguez-Reinoso, F.; Rouquerol, J.; Sing, K. S. W. Physisorption of Gases, with Special Reference to the Evaluation of Surface Area and Pore Size Distribution (IUPAC Technical Report). *Pure Appl. Chem.* **2015**, *87*, 1051−1069.
(26) Möller, K.; Bein, T. Talented Mesoporous Silica Nanoparticles. *Chem. Mater.* **2017**, *29*, 371−388.
(27) Pantaleo, G.; La Parola, V.; Deganello, F.; Singha, R. K.; Bal, R.; Venezia, A. M. Ni/CeO_2 catalysts for methane partial oxidation: Synthesis driven structural and catalytic effects. *Appl. Catal., B* **2016**, *189*, 233−241.
(28) Wang, G.; Wang, H.; Zhang, H.; Zhu, Q.; Li, C.; Shan, H. Highly selective and stable NiSn/SiO_2 catalyst for isobutene dehydrogenation: Effects of Sn addition. *ChemCatChem* **2016**, *8*, 3137−3145.
(29) Hengne, A. M.; Samal, A. K.; Enakonda, L. R.; Harb, M.; Gevers, L. E.; Anjum, D. H.; Hedhili, M. N.; Saih, Y.; Huang, K.-W.; Basset, J.-M. Ni−Sn-Supported ZrO_2 Catalysts Modified by Indium for Selective CO_2 Hydrogenation to Methanol. *ACS Omega* **2018**, *3*, 3688−3701.
(30) Hou, Z.; Yokota, O.; Tanaka, T.; Yashima, T. Surface properties of a coke-free Sn doped nickel catalyst for the CO_2 reforming of methane. *Appl. Surf. Sci.* **2004**, *233*, 58−68.
(31) Onda, A.; Komatsu, T.; Yashima, T. Preparation and Catalytic Properties of Single-Phase Ni−Sn Intermetallic Compound Particles by CVD of $Sn(CH_3)_4$ onto Ni/Silica. *J. Catal.* **2001**, *201*, 13−21.

https://doi.org/10.1021/acs.iecr.1c02193
Ind. Eng. Chem. Res. 2021, 60, 18684−18694